Ping Guo[1]
Department of Mechanical Engineering,
Northwestern University,
2145 Sheridan Road,
Evanston, IL 60208
e-mail: pingguo2009@u.northwestern.edu

Yong Lu
State Key Laboratory of Automotive
Safety and Energy,
Tsinghua University,
Beijing 100084, China
e-mail: luy05@mails.tsinghua.edu.cn

Pucheng Pei
State Key Laboratory of Automotive
Safety and Energy,
Tsinghua University,
Beijing 100084, China
e-mail: pchpei@mail.tsinghua.edu.cn

Kornel F. Ehmann
Department of Mechanical Engineering,
Northwestern University,
2145 Sheridan Road,
Evanston, IL 60208
e-mail: k-ehmann@northwestern.edu

Fast Generation of Micro-Channels on Cylindrical Surfaces by Elliptical Vibration Texturing

Micro-structured surfaces are assuming an ever-increasing role since they define the ultimate performance of many industrial components and products. Micro-channels, in particular, have many potential applications in micro-fluidic devices, micro heat exchangers, and friction control. This paper proposes an innovative vibration-assisted machining method to generate micro-channels on the external surface of a cylinder. This method, referred to as elliptical vibration texturing, *was originally developed by the authors to generate dimple patterns. It uses the modulation of the depth-of-cut by tool vibrations to create surface textures. The most promising features of the proposed method are its high efficiency, low cost, and scalability for mass production. It is shown that with proper combinations of the process parameters the created dimples start to overlap and form channels. An analytical model is established to predict channel formation with respect to the overlapping ratios of the dimples. Channel formation criteria and expressions for channel geometries are given along with a channel generation map that relates channel geometry to the process parameters. Experimental results are given to verify the model. A further example of micro-pattern generation is also given to showcase the flexibility of the process.* [DOI: 10.1115/1.4027126]

Keywords: elliptical vibration cutting, micro-channel, micro-dimple, surface texturing

1 Introduction

Micro-structured surfaces represent a new trend of promising technologies for enhancing the functionality and performance of industrial components. Surface micro-structures, when carefully designed, can alter the optical, biological, tribological, and thermal properties of the original surfaces. Comprehensive reviews have been made on micro-structured surfaces and on their theories, applications, and manufacturing techniques [1,2]. To name a few applications, micro-pillar arrays are a classic example to achieve superhydrophobic surface properties, which are bio-inspired features from the structure of lotus leaves [3]. Undulated surfaces help in decreasing friction and wear by reducing ploughing and are also instrumental in trapping wear particles in the gaps [4]. Micro-prism arrays are used for enhanced reflection of light, which are very common in the traffic road signs and in every LCD screen.

Micro-channels are, particularly, widely utilized in various applications of micro-fluidic devices [5], micro heat exchangers [6], and friction reduction [7]. Most applications are based on planar substrate surfaces, since conventional generation methods for micro-channels including laser ablation and lithography-based machining were originally limited to 2D surfaces. One example of micro-channels (or grooves) on 3D surfaces is the spiral grooves on journal bearings for friction reduction [8]. The spiral grooves serve as oil pockets to decrease abrasive wear. Results have shown an over two-times decrease in wear when compared to untextured journal bearings [9].

Many efforts have been made towards extending the 3D capability of existing manufacturing processes (e.g., mechanical machining, laser ablation, lithography-based machining, etc.). Takeuchi et al. [10] developed a sophisticated six-axis NC machining center for micro-grooving on sculptured surfaces for optical devices. Holmes et al. [11] introduced projection ablation methods, such as synchronous image scanning and half-tone masks, to achieve 3D structuring with complex profiles. Groenendijk [12] integrated a five-axis motion stage to achieve laser ablation on free-form surfaces while Hao et al. [13] developed a rolling-exposure lithography technique to create large-scale 3D microstructures on cylindrical objects. Adams et al. [14] used focused ion beam sputtering to create micro-grooving tools and managed to machine 13 μm wide, 4 μm deep, helical grooves on cylindrical workpieces. Li et al. [15] studied micro-cutting of V-shaped grooves for roller nano-imprinting. They optimized the cutting tool design and process parameters for minimized burr formation. All these studies have shown significant progress in solving difficulties in the creation of microstructures on 3D surfaces. They, however, were limited in industrial production by their complicated mechanisms, expensive equipment, low throughput, or material restrictions.

The elliptical vibration-assisted cutting technique has also been applied to micro-grooving and, especially, for cutting brittle and hard-to-cut materials. Lee et al. [16] applied two-dimensional ultrasonic vibrations to the micro-grooving of glasses and planar lightwave circuits. They achieved a better groove shape. Liu et al. [17] studied ductile mode cutting in grooving of tungsten carbide. They have found that the critical depth of cut for the transition from the ductile to the brittle cutting mode is increased several times with the aid of one-dimensional ultrasonic vibrations. Machined micro-channels and quadrangular pyramids with significantly improved form accuracy using elliptical vibration cutting were demonstrated by Kim and Loh [18]. Suzuki et al. [19] modulated the exciting voltage in elliptical vibration cutting (EVC) to control the envelope profiles of the tool trajectories to create various textured grooves.

[1]Corresponding author.

Contributed by the Manufacturing Engineering Division of ASME for publication in the Journal of Manufacturing Science and Engineering. Manuscript received July 1, 2013; final manuscript received March 1, 2014; published online May 21, 2014. Assoc. Editor: Tony Schmitz.

This paper proposes an innovative machining method for the fast generation of micro-channels: the *elliptical vibration texturing* process. It utilizes the vibrations of the cutting tool, when applied in the turning operation, to create controlled parallel micro-channels on the external surface of a cylinder. The newly developed process, based on the elliptical vibrations of the cutting tool, retains the same general principles as the traditional EVC process [20]. It, however, differs in the cutting mechanism. The EVC process utilizes the vibration of the tool to improve the local cutting conditions, e.g., to decrease the effective chip thickness and to reduce the contact time between the tool and the workpiece, while the elliptical vibration texturing process uses the modulation of the cutting depth by the tool vibrations to create surface textures. According to the definition of the horizontal speed ratio (HSR) in Ref. [20], EVC processes create overlapping cutting trajectories for which HSR is less than one. The proposed method works in the range where HSR is greater than one, to generate non-overlapping tool trajectories. The vibrations in the depth-of-cut direction dictate the texturing process, while the vibrations in the cutting direction vary the cutting speed, (in the continuous cutting mode, $HSR > 1$). Compared with the fast tool servo (FTS) technology (one-dimensional), such as Ref. [21], the proposed method adds an additional degree-of-freedom in the cutting direction offering more flexibility in controlling the texture profile, it is fast and, as such, saves time and reduces costs in industrial applications.

The most promising features of the proposed method are its high efficiency, low cost, and scalability for mass production. Often the bottlenecks for the applications of micro-structured surfaces in consumer products are exactly in these three areas. The elliptical vibration texturing process is about three orders of magnitude faster than other commonly applied manufacturing methods. Laser ablation and conventional mechanical machining usually take several seconds to create a dimple. For example, when using elliptical vibration texturing more than 25 thousand dimples are generated in a second thanks to the ultrasonic vibration frequency of the tool. The cost of the process is no different than in the conventional machining method, since the process can be easily incorporated into conventional lathes or three axes computer numerical control (CNC) machines. No expensive or specialized machines are required. The scalability of the process manifests itself in two areas: (a) it can be applied to large areas as compared to lithography-based methods and (b) it is suitable for production in large quantities.

The paper starts with an introduction to the elliptical vibration texturing process along with the experimental setup for the process. Then, the theoretical analysis of micro-dimple and micro-channel generation is given. Experimental results are presented and compared to the analysis. Finally, the flexibility of the process is demonstrated by extending the method to the creation of more complex micro-patterns. It should be noted that the proposed method has the capabilities to process a wide selection of materials, although in the current paper only aluminum is used as a model material to verify of the geometric and kinematic models of the process.

2 Elliptical Vibration Texturing

The authors have developed the elliptical vibration texturing method designed to create micro-dimple arrays on cylindrical surfaces [22,23]. This process can be extended to generate spiral micro-channels on curved surfaces by carefully choosing the process parameters. All parallel channels are created simultaneously with the proposed method, which can be "imagined" as the generation of a multi-threaded rod in a single-path cutting operation. The detailed analysis, which is the focus of this paper, will be given later. However, for the sake of completeness of the concept, the original process is briefly introduced first.

2.1 Principle of Operation. The elliptical vibration texturing process originated from the authors' previous work that has introduced the concept of the surface-shaping system [24]. A periodic tertiary motion is applied to the cutting tool in the depth-of-cut direction besides the primary (cutting) and secondary (feed) motions. When applied to cylindrical turning, a kind of fast tool servo device could be utilized to realize the concept. The so-called fast tool servo devices typically utilize a piezoelectric actuator to obtain high precision motions up to a several hundred hertz bandwidth [25]. One example of this concept is applied to texturing the external surfaces of journal bearings to reduce friction [26]. However, the efficiency of this original design is not satisfactory. The cutting speed is also limited by the frequency of the tertiary motion, since the variation motion in the depth-of-cut has to be synchronized with the cutting motion. The low frequency (several hundred hertz) of the tertiary motion results in a low cutting speed, which deteriorates the surface finish.

All these concerns can be alleviated by adopting the ideas that were introduced by the concept of ultrasonic elliptical vibration cutting. Moriwaki and Shamoto [27] first applied the elliptical vibration cutting process with the aim of reducing the cutting force and the chip thickness. The key component of their device was a well-designed vibrator, which could deliver an elliptical tool trajectory at an ultrasonic frequency. It utilizes the coupled resonant vibrations of the tool holder structure to achieve high vibration amplitudes in the ultrasonic frequency range. Later, various studies have been dedicated to the further development of this process, including steel cutting using diamond tools [28,29], tungsten carbide machining [30,31], ductile cutting of brittle materials [32,33], etc.

In the proposed elliptical vibration texturing process, a similar elliptical trajectory is applied to the cutting tool as in the EVC process. The two-dimensional vibrations can be decomposed into two perpendicular vibrations in the cutting direction and the direction perpendicular to the workpiece surface. The vibrations in the depth-of-cut direction dictate the texturing process. The vibrations in the cutting direction add an additional means of controlling the geometry of the generated structures, e.g., the convexity of the bottom shape of the dimples.

As summarized in Fig. 1, the resultant tool trajectories are the result of the combined motions of the tool's elliptical vibrations,

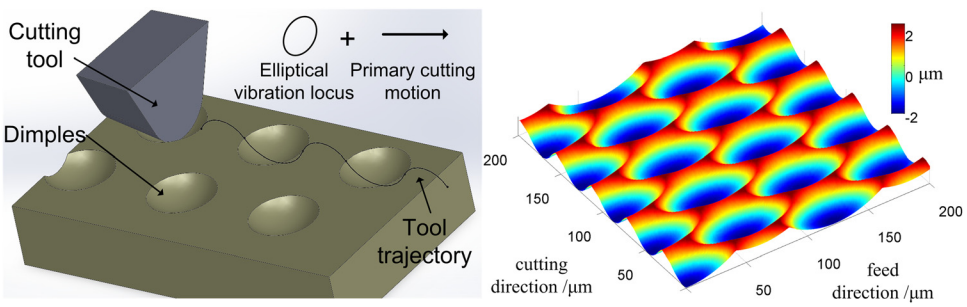

Fig. 1 Schematic of the elliptical vibration texturing process

the cutting and feed motions, which create periodic variations in the surface profile. When the process is applied to the turning operation, the tertiary motion lies in the plane perpendicular to the axis of the cylindrical workpiece. The efficiency of the process is determined by the vibration frequency of the tool, which is in the ultrasonic frequency range. The cutting velocity (workpiece rotation speed) is also increased accordingly due to the high frequency vibration. For better understanding, an example of the generated surface is also illustrated in Fig. 1. If the tool's tertiary motion is predetermined, the arrangement of the dimple patterns is influenced by the process parameters (cutting speed and feedrate). The dimple shape is determined by tool geometry.

2.2 Tertiary Motion Generator. The tertiary motion generator is designed to generate an elliptical trajectory at a fixed ultrasonic frequency. The device utilizes the coupled resonant vibrations of the structure to achieve high vibration amplitudes. It works at one distinct frequency, which is the intrinsic feature of the mechanical structure. The computer aided design (CAD) model of the design is shown in Fig. 2. Two standard Langevin transducers are held together at one end with a flexure structure. The angle between the two transducers is 60 deg. Through modal analysis, two distinctive vibration modes associated with the flexure can be identified. In one mode, the flexure vibrates symmetrically to create a normal motion in the depth-of-cut direction, while in the other mode the flexure vibrates asymmetrically to create a shear motion in the cutting direction. The structure is carefully designed in a manner to assure that the resonant frequencies of the above two modes are coincident. So, both modes are excited at a nearly identical frequency with a certain phase shift, resulting in the elliptical trajectories. The detailed description of the design has been discussed in the authors' previous work [22].

2.3 Experimental Setup. Elliptical vibration texturing experiments were performed in a turning operation to demonstrate micro-structure generation on the external surfaces of cylindrical workpieces. The machining setup, shown in Fig. 3, was arranged on a customized micromachining setup in the form of a vertical lathe. The cutting tool used was a single crystal diamond insert with a nose radius of 200 μm. The tool was oriented with respect to the workpiece at a zero rake angle and a 7 deg clearance angle. The tertiary motion generator is excited at 27.4 kHz. The vibrations amplitudes were 9.0 μm in the depth-of-cut direction and 9.0 μm in the cutting direction, respectively. The phase angle, defined as the phase shift angle between two sinusoidal vibrations in the two orthogonal directions [22], was 12 deg. The orientation of the elliptical tool trajectory, which is characterized by the tilt angle between the major axis of the ellipse and the depth-of-cut direction, was measured to be 40 deg. The workpieces were 3 mm in diameter made of Aluminum 2011.

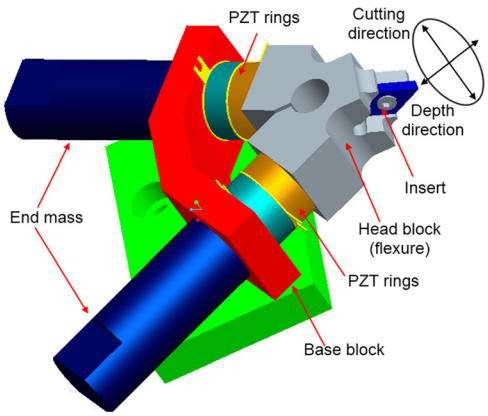

Fig. 2 3D model of the tertiary motion generator

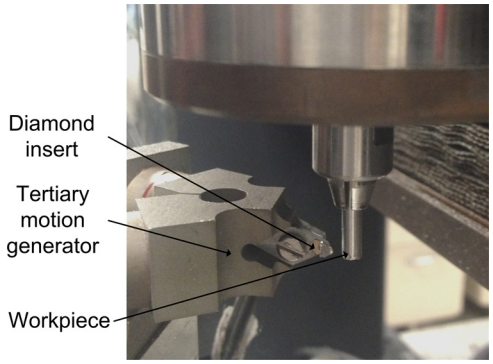

Fig. 3 Experimental setup

3 Theoretical Analysis of Micro-channel Generation

In this section, a theoretical analysis is carried out first on the dimple pattern geometry and the dimple shape itself. This analysis constitutes the basis for the development of the channel generation methodology. Channels are formed when the dimple gaps decrease to a point where the dimples start to overlap in one direction. The overlapping ratio of the dimple areas will be introduced to predict channel formation. For the derivation of an analytical expression for the overlapping ratio, the dimple geometry is approximated by a diamond shape, whose two diagonal lengths match the dimple's height and width. The channel geometry is defined and theoretically calculated. A channel generation map is given for the prediction of channel formation under different process parameter conditions. Combining both the channel geometry expressions and the channel generation map, the proper process parameters are determined given the desired channel shape.

3.1 Dimple Array Geometric Definition. Typical dimple patterns and their geometrical relationships are depicted in Fig. 4. The horizontal direction is the feed direction in the turning operation, while the vertical direction is the cutting direction. If the vibration trajectory and frequency are predetermined, the relative positions of the dimples are determined by the process parameters, i.e., the spindle speed and feedrate.

The ratio of the excitation frequency of the tool vibration and the spindle speed is defined as λ, the "cutting frequency ratio." It can be separated into an integer K and a fractional part, ε, i.e.

$$\lambda = \frac{60f}{N} = K + \varepsilon \tag{1}$$

where f is the excitation frequency, and N is the spindle rotation speed (RPM). K determines the number of dimples around the circumference of the workpiece, while ε decides the phase shift distance, δ, between two consecutive columns of dimples. The phase shift can be expressed as:

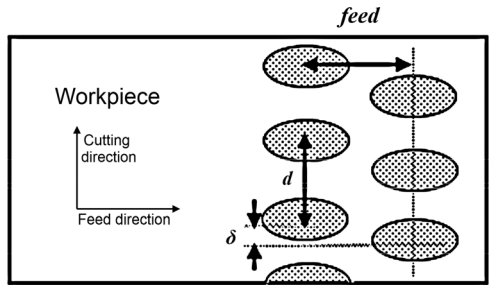

Fig. 4 Dimple array geometry definition

$$\delta = \frac{2\pi R_0 \varepsilon}{\lambda} \tag{2}$$

where R_0 is the radius of the workpiece.

The dimple separation distance, d, along the cutting direction is defined by

$$d = \frac{2\pi R_0}{\lambda} \tag{3}$$

The gap in the lateral direction, as indicated in Fig. 4, is just the *feed*, which is defined in the unit of length per revolution. All these characteristic variables are only depending on the proper combination of process parameters, spindle speed and feedrate, in Eq. (1).

3.2 Geometric Analysis of Channel Generation. When the *feed* and/or δ are decreasing, the dimples start to overlap each other. As shown in Fig. 5, depending on the direction in which overlapping occurs, the channels are formed in one of three possible directions to be denoted as *Mode I*, *Mode II*, and *Mode III*. *Mode I* and *Mode II* channels are formed by connecting dimples in adjacent columns. *Mode I* channels lie in the first and third quadrants; while *Mode II* channels lie in the second and fourth quadrants. *Mode III* channels form by connecting dimples in every second column. Representative channel shapes for each mode are shown in Fig. 5. Channel formation is related to the process parameters, as well as the tool geometry. The criteria for channel generation need to be determined to answer questions whether certain process parameter combinations will generate channels and which channel mode is in effect.

The dimple shape itself is a replica of the tool geometry. It is also determined by the tool vibration trajectories. If the elliptical motion can be decomposed into two sinusoidal functions in the cutting and depth-of-cut direction and expressed by

$$\begin{aligned} X &= A_x \sin(\omega_t t + \varphi_x) \\ Y &= A_y \sin(\omega_t t) \end{aligned} \tag{4}$$

where X is the tool displacement in the cutting direction, Y in the depth-of-cut direction, ω_t is the angular velocity of the vibrations, φ_x is the phase shift between the two motions and A_x and A_y represent one half of the vibration amplitudes. Then, one can define the effective feature depth, considering the vibration amplitudes of the cutting tool, by a piecewise function

$$t_{\text{eff}} = \begin{cases} 2A_y & DOC > A_y \\ DOC + A_y & DOC < A_y \end{cases} \tag{5}$$

where *DOC* is the nominal depth-of-cut set by the lathe (without considering the tool's vibrations).

The effective feature depth is the actual depth of the generated dimples or channels. When the nominal *DOC* is smaller than one half of the axial vibration amplitude, as shown by Case 1 in Fig. 6, the effective feature depth is just the distance from the original workpiece surface to the lowest point on the tool's vibration trajectory. When the nominal *DOC* exceeds A_y (Case 2 in Fig. 6), the effective feature depth is the peak-to-peak amplitude of the tool's vibration ($2A_y$).

The dimple width is derived as

$$W = 2\sqrt{R_n^2 - (R_n - t_{\text{eff}})^2} \tag{6}$$

where R_n is the tool noise radius.

The dimple length is influenced by both the tool vibration and the nominal cutting velocity (spindle speed). To calculate the dimple length, the coordinates of two points, t_1 and t_2, need to be found in Fig. 6. According to the figure, t_1 is a particular solution in the range of 0 and $\pi/2\omega$ of the equation

$$A_y \sin(\omega_t t_1) = t_{\text{eff}} - A_y \tag{7}$$

then t_2 is another solution of Eq. (7) and is defined by

$$t_2 = -\omega_t t_1 - \pi \tag{8}$$

The dimple length then can be expressed as

$$L = 2A_x \cos(\omega t_1) \sin(\varphi_x) + \frac{2\pi R_0 N}{60}(t_1 - t_2) \tag{9}$$

When the *DOC* is greater than A_y (Case 2 in Fig. 6), the effective feature depth is constant at $2A_y$, and the solution for Eq. (9) reduces to

$$L = \frac{2\pi R_0 N}{60f} \tag{10}$$

which coincides with the expression for the dimple separation distance, d, in Eq. (3).

To predict channel formation a process-dependent variable to be referred to as the "overlapping ratio" of the dimples will be introduced. To simplify the calculation of the overlapping ratio, the actual dimple geometry/area will be approximated by a diamond shape (Fig. 7(*a*)). The half diagonal length in the circumferential (vertical) direction, $L/2$, will be denoted by b, the half diagonal length in the axial (horizontal) direction, $W/2$, by a, and the height of the diamond by H. It should be noted that the actual dimple shape is an approximate ellipse, so this assumed inscribed diamond is an underestimate of the dimple shape area.

Since the analysis procedure to be presented is very similar for each mode, only *Mode I* will be presented in detail. The schematic of dimple overlap layout in *Mode I* is plotted in Fig. 7(*a*), along

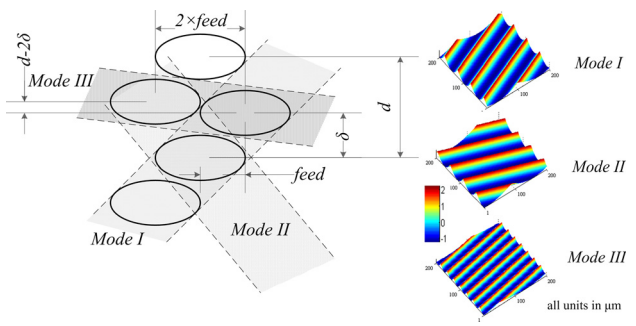

Fig. 5 Channel generation schematics and simulated channels in different modes

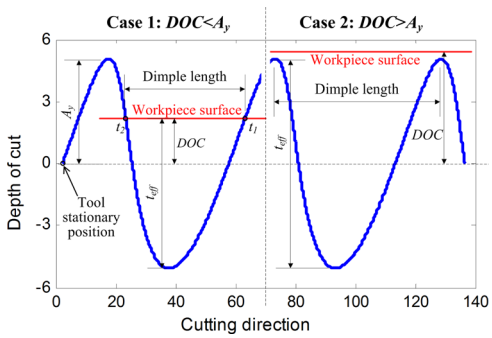

Fig. 6 Effective feature depth and dimple length diagram

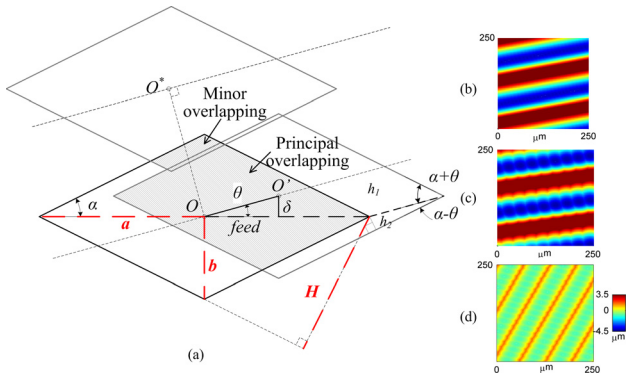

Fig. 7 Channel formation: (*a*) dimple overlap diagram (*b*) well-formed channels (*c*) small principal overlapping ratio and (*d*) non-zero minor overlapping ratio

with representative examples of channel formation based on different overlapping ratios in Figs. 7(*b*)–7(*d*). The variables in the figure that are related to the process parameters are the horizontal gap, *feed,* and the phase shift distance, δ. The value of *feed* equals to the value of the feedrate. According to Eqs. (1) and (2), δ is determined by the workpiece radius and the cutting frequency ratio, which is the ratio between the tool vibration frequency and the spindle speed.

According to Fig. 7(*a*), one can define the overlapping ratio, *r*, as the intersection area of two overlapping diamond shapes divided by the area of the diamond itself. The overlapping ratio is a good indicator of how well a channel is formed. Intuitively, a larger overlapping ratio, *r*, results in a better formed channel.

Two important angles in the figure are defined, which are the aspect ratio angle of the diamond

$$\alpha = \arctan\left(\frac{b}{a}\right) \tag{11}$$

and the channel orientation angle

$$\theta = \arctan\left(\frac{\delta}{feed}\right) \tag{12}$$

The overlapping ratio, *r,* for *Mode I* is then derived as

$$r_1 = \left(1 - \frac{h_1}{H}\right) \cdot \left(1 - \frac{h_2}{H}\right) \tag{13}$$

where

$$h_1 = \sqrt{\delta^2 + feed^2} \cdot \sin(\alpha + \theta) \tag{14}$$

$$h_2 = \sqrt{\delta^2 + feed^2} \cdot \sin(|\alpha - \theta|) \tag{15}$$

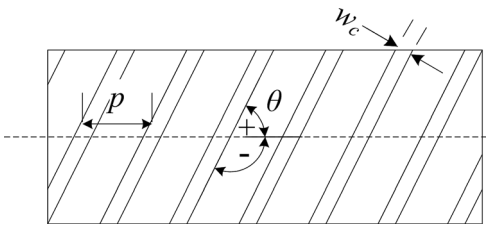

Fig. 8 Schematic of "multi-threaded" spiral channels

Table 1 Expressions for channel geometries

Mode	Channel orientation θ	Channel width w_c	Pitch p
I	$\arctan\left(\frac{\delta}{feed}\right)$		$d\cot(\lvert\theta\rvert)$
II	$-\arctan\left(\frac{d-\delta}{feed}\right)$	$2b\sin(\lvert\theta\rvert)$ $\lvert\theta\rvert > \alpha$ $2a\cos(\theta)$ $\lvert\theta\rvert \le \alpha$	$d\cot(\lvert\theta\rvert)$
III	$-\arctan\left(\frac{d-2\delta}{2feed}\right)$		$\frac{1}{2}d\cot(\lvert\theta\rvert)$

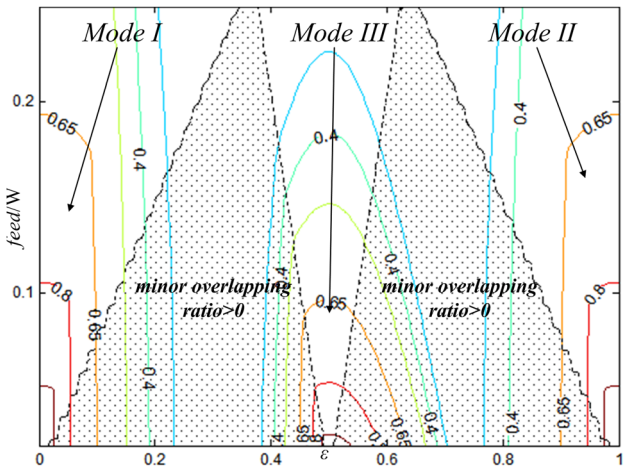

Fig. 9 Generalized channel generation map

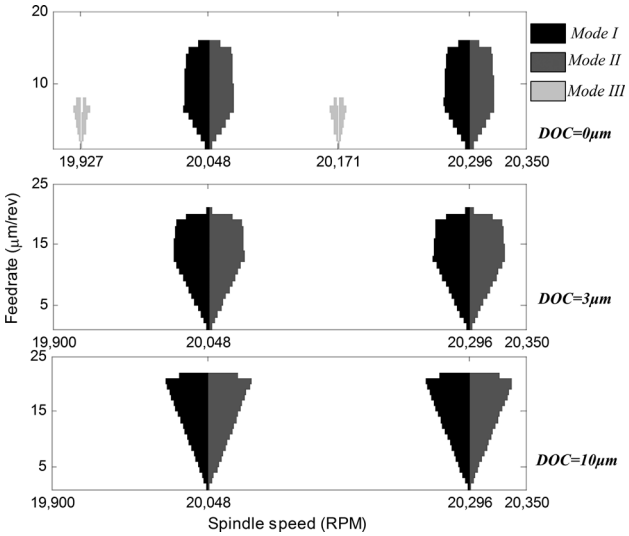

Fig. 10 Channel generation map

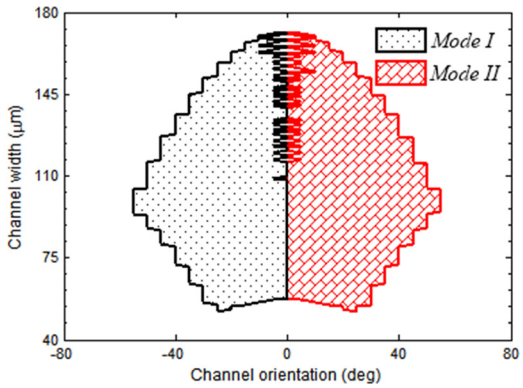

Fig. 11 Feasible region for channel generation

In a similar manner, overlapping ratios can be defined for *Mode II* and *Mode III* channels as well. The maximal ratio of the three determines the channel mode (Fig. 5), and will be referred to as the *"principal overlapping ratio."* A channel will form in the dashed line direction, indicated by the orientation angle, θ. The closest dimple in the adjacent channel is located at center O^*, where OO^* is the distance between two channels. The overlapping ratio between these two adjacent dimples (O and O^*) is another determining factor for channel formation and will be referred to as the *"minor overlapping ratio."* The minor overlap of the dimples can be viewed as a "disturbance" to the principal channel mode, which deteriorates the channel formation process. Ideally, a smaller minor overlapping ratio results in better separated and well-defined channel formation. Since the simplified dimple geometry is inscribed in the actual dimple shape, it is an underestimate of the actual dimple size. The threshold for the minor overlapping ratio can be set at zero to ensure a minimal overlap between two neighboring channels. A zero minor overlapping ratio condition is satisfied by

$$d\cos(\theta)\sin(\alpha+\theta) > H, \quad \text{or} \qquad d\cos(\theta)\sin(|\alpha-\theta|) > H \tag{16}$$

In general, a larger principal overlapping ratio gives a smoother finish for a channel. A minimal value can also set on the principal overlapping ratio for acceptable channel formation. An example of ill-formed/incomplete channels due to a too small principal overlapping ratio is shown in Fig. 7(*c*). The principal and minor overlapping ratios are 0.52 and 0, respectively. For comparison, the baseline showing well-formed channels is plotted in Fig. 7(*b*) with overlapping ratios of 0.82 and 0. A non-zero minor overlapping ratio deteriorates the principal channel mode. An example of incomplete channels due to a non-zero minor overlapping ratio is plotted in Fig. 7(*d*) with a principal ratio of 0.70 and a minor ratio of 0.17.

Channel geometry can be derived from the process parameters. The spiral micro-channels generated by the elliptical vibration texturing process are in concept very similar to a multi-threaded screw. The schematic of the geometry is shown in Fig. 8. The major geometrical parameters include the channel width w_c, the pitch p, and the orientation angle θ that is defined as the angle between the channel and the axis of the cylinder. The channels are generated by extending the original dimple generation method [23]. The process parameters are carefully chosen to overlap the dimples to form consecutive channels.

The channel geometries for *Mode I* channels can be obtained according to Fig. 7(*a*). The channel orientation angle is just the angle θ in the figure, where the sign of the angle is defined according to Fig. 8. The expression for θ is given by Eq. (12).

The channel width is derived from

$$w_c = \begin{cases} 2b\sin(|\theta|) & |\theta| > \alpha \\ 2a\cos(\theta) & |\theta| \le \alpha \end{cases} \tag{17}$$

The pitch, p, of the spiral channels is the distance between the adjacent channels in the feed direction, which is given by

$$p = \frac{2\pi R_0 N}{60f}\cdot\cot(|\theta|) = d\cot(|\theta|) \tag{18}$$

where d is the dimple separation distance as defined in Fig. 5.

The lead of the spiral channels, similar to the definition for threads, is the distance along the feed direction over a complete revolution of a single channel and is given by $K\cdot p$, where K is the integer part of the cutting frequency ratio, λ, as defined by Eq. (1) and it determines how many separate channels are created.

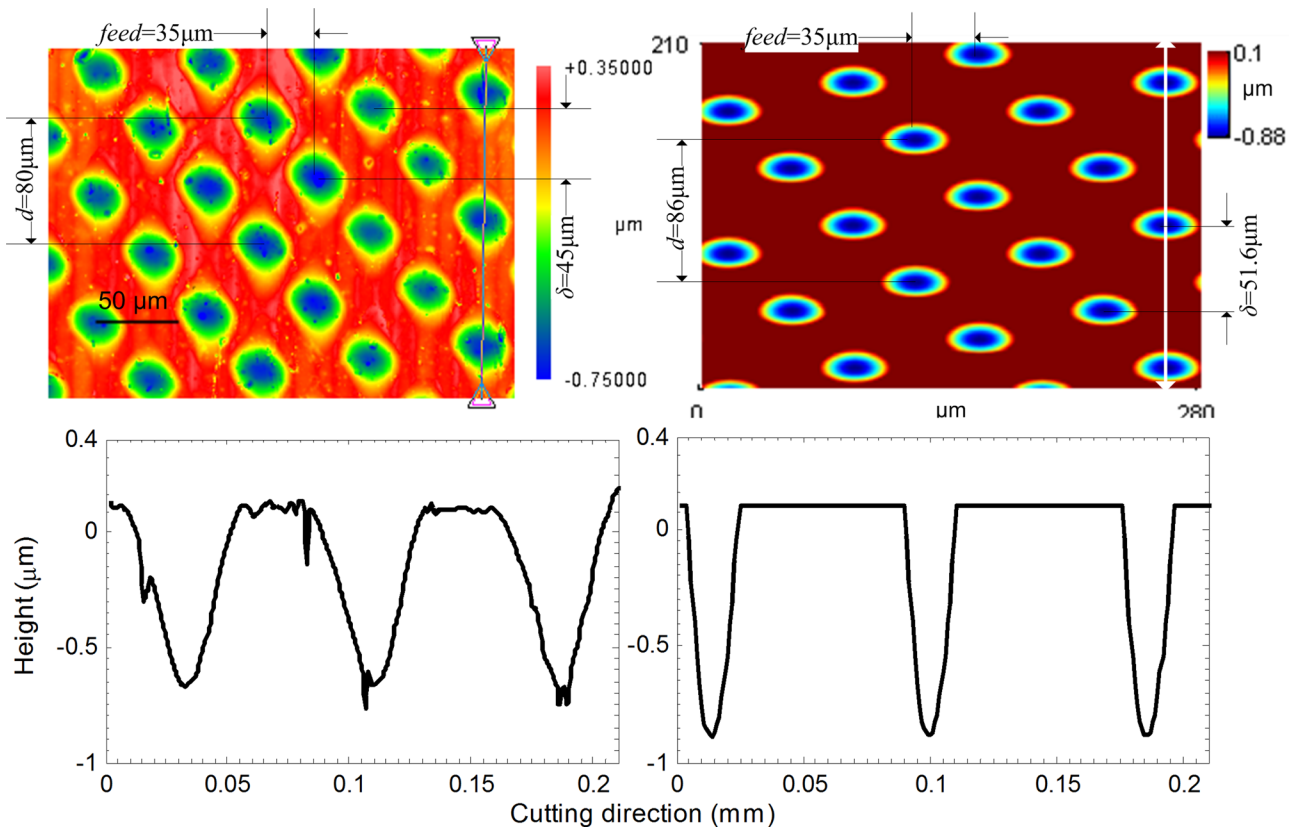

Fig. 12 Comparison between experiments and simulation of surface topography and profiles for dimple arrays

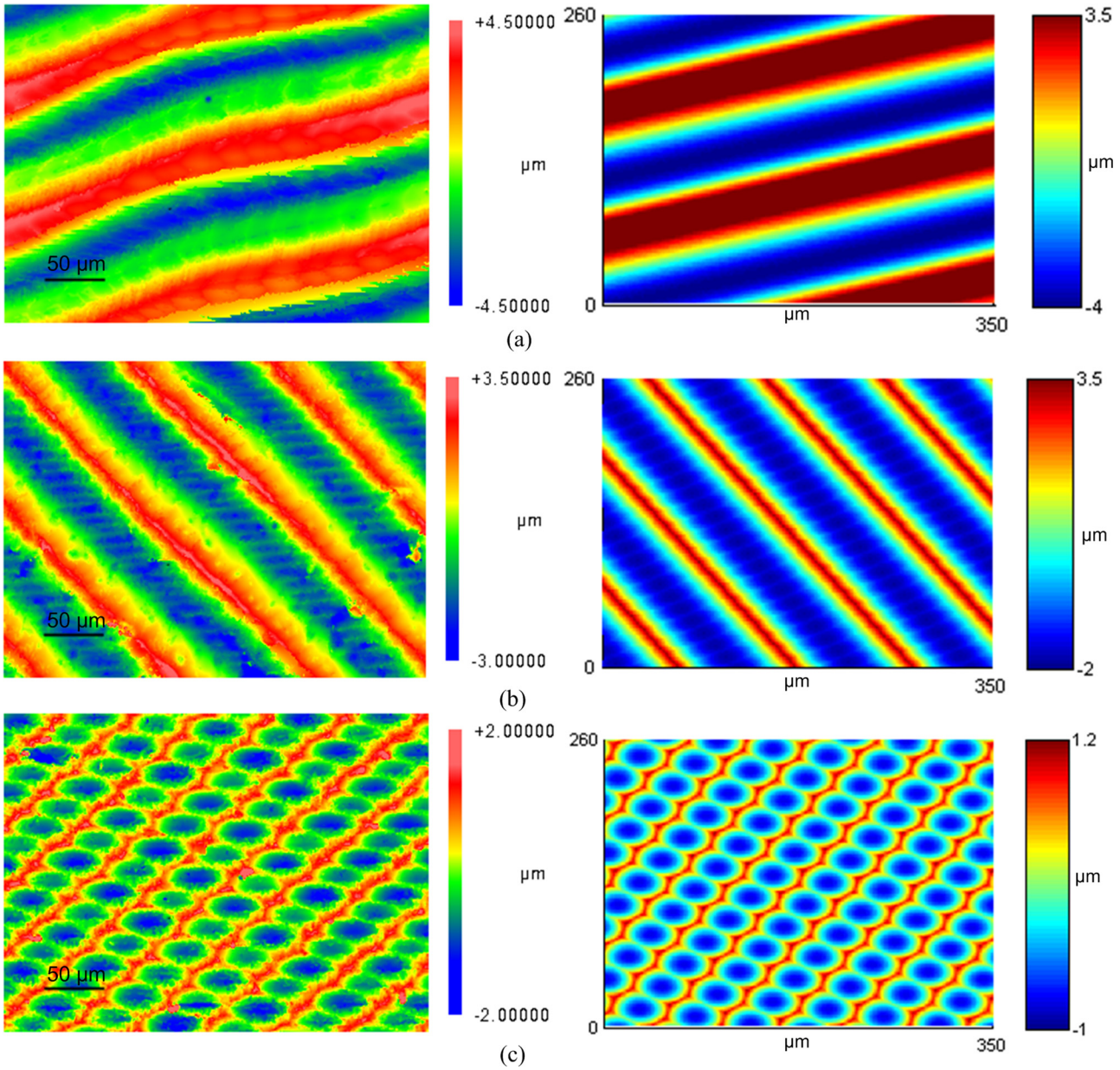

Fig. 13 Examples of generated and simulated surface topography of micro channels: (*a*) *Mode I* channels (N = 20,044 RPM, *feed* = 10 μm, *DOC* = 3 μm), (*b*) *Mode II* channels (N = 20,072 RPM, *feed* = 10 μm, *DOC* = 3 μm), and (*c*) unsuccessful *Mode III* channels (N = 19,906 RPM, *feed* = 10 μm, *DOC* = 3 μm)

Similar analyses can be applied to *Mode II* and *Mode III* channels as well. The results are summarized in Table 1.

3.3 Channel Generation Map. Channel formation characteristics can be calculated based on the thresholds of the principal and minor overlapping ratios for various process parameters (spindle speed, feedrate, and *DOC*). As analyzed in the previous section, for successful channel generation the principal overlapping ratio should exceed a threshold value. This threshold value is set to be 0.65 for a smooth channel formation based on the results from the experiments and simulations. The condition for the minor principal ratio is set at 0 for minimal overlapping in the cross-channel direction. As a generalized example in Fig. 9, the X axis is ε, the non-dimensional variable representing the spindle speed as determined by the ratio of the tool vibration frequency and the spindle speed [(Eq. (1)]. The Y axis is another non-dimensional quantity, which is a function of the feedrate, vibration amplitudes, *DOC*, etc. The figure shows the contour plot of the values of the principal overlapping ratio for the three channel modes, where each mode is dominant in a specific range of ε. For example, when ε is between 0 and 0.3 the overlapping area in the *Mode I* direction is the largest among the three modes. The principal overlapping ratio then is defined in *Mode I* and is calculated according to Eq. (13). The shaded areas in the figure correspond to the conditions where the minor overlapping ratio is greater than zero. According to the channel generation criteria, only when the principal overlapping ratio exceeds 0.65 and the minor overlapping ratios remains 0, a channel will be successfully formed. This condition is indicated in the figure by the area enclosed by the contour line labeled as 0.65, excluding the shaded area.

For the specific case used in the experiments described below, the channel generation maps are explicitly evaluated for the given spindle speed, feedrate and *DOC* and plotted in Fig. 10. For each combination of feedrate, spindle speed, and *DOC*, the principal

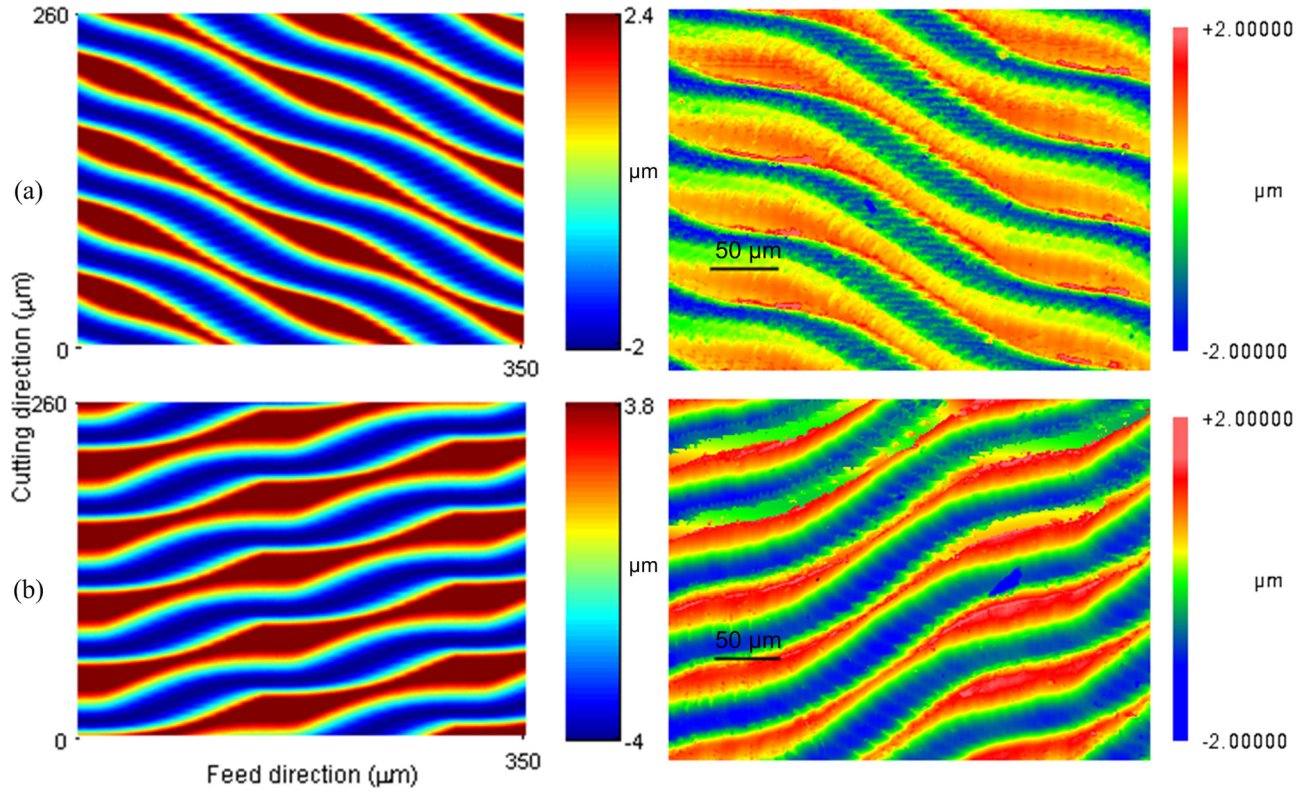

Fig. 14 Influence of the spindle speed variation: (*a*) *Mode II* channels (N = 10,029 RPM, *feed* = 10 μm, *DOC* = 3 μm) and (*b*) *Mode I* channels (N = 8998 RPM, *feed* = 1010 μm, *DOC* = 3 μm)

and minor overlapping ratios are calculated and the channel formation is determined accordingly. These maps are corresponding to the experimental conditions as described in the experimental setup section. The workpiece has a diameter of 3 mm, the cutting tool has a nose radius of 200 μm, the vibration amplitudes are 9.0 μm in both directions with a phase angle [22] of 12 deg and the exciting frequency is at 27.4 kHz. The variables are the spindle speed, feedrate, and *DOC*. The spindle speed is chosen from 19,900 to 20,350 RPM, the feedrate is kept between 1 and 25 μm/rev, and the nominal *DOC* is chosen at 0 μm, 3 μm (less than half of the vibration amplitude), and 10 μm (greater than the vibration amplitude. From the map, it can be concluded that: (1) only the right combinations of the spindle speed and the feedrate will generate micro-channels. Neither variable is a determining factor for channel generation. (2) The map repeats itself along the spindle speed axis, so it is a periodic function of the spindle speed. Within a period, the spindle speed influences the channel mode, while between periods the spindle speed determines the number of parallel channels generated on the cylinder.

By linking the channel geometry expressions and the channel generation map, the proper process parameters can be determined given the desired channel shape. From the channel generation map in Fig. 10, the successful channel formation mode can be predicted given the spindle speed, feedrate and *DOC*. The resultant channel geometries (orientation and width) can be calculated according to Table 1. This step links the process parameters to the channel geometry. The calculation is done for every possible channel formation condition. An inverse relationship then can be established by reversing the link, which outputs the required process parameters from the channel geometry. It should be noted that this mapping from channel geometry to the process parameters is neither injective nor surjective, i.e.: (1) not all combinations of parameters will generate a channel; (2) not all channel geometries are feasible; and (3) multiple process parameters could generate the same channel geometry. As an example, a feasible region for channel generation is given in Fig. 11. The spindle speed is chosen between 10,000 and 30,000 RPM, the feedrate is from 1 to 25 μm/rev and the *DOC* is kept at 3 μm, i.e., the same as for the experimental conditions.

4 Experimental Verification

The experimental setup has been described before. The first set of experiments was aimed to verify the dimple pattern analysis given in Sec. 3.1. The spindle speed was set to 15,000 RPM, the feedrate was kept at 35 μm/rev and the nominal *DOC* was -2 μm (2 μm above the workpiece surface). The results are shown in Fig. 12. The generated surface topography and surface profile along the cutting direction are plotted on the left, while the corresponding simulation results are illustrated on the right. The measured and theoretical values of the *feed*, phase shift distance, δ, and dimple separation distance, d, are compared and listed in the figure. The elliptical vibration texturing process produces the dimple arrays as predicted. This is the foundation step to overlap the dimples to generate channels.

Building on the analysis on channel formation, three examples of comparison between the experimental results and simulations are given in Fig. 13, including good and incomplete channel formation. The input parameters for the experiments as well as the simulation are kept the same as listed in the caption of the figure. According to the results, the experiments match the simulation.

For the *Mode I* channels in Fig. 13(*a*), the major overlapping ratio is calculated to be 0.82; while the minor overlapping ratio is 0. The channel orientation angle is estimated to be 12.7 deg, and the channel width is 83.5 μm. For the *Mode II* channels in Fig. 13(*b*), the major and minor overlapping ratios are 0.75 and 0, respectively. The channel orientation angle is -47.5 deg (towards the left). The channel width is 80.0 μm. Based on the channel generation criteria, good formation of channels is expected for these two cases. The channel geometries are hard to quantify accurately, since the channel orientation angle depends on the placement of the workpiece and there is no clear inflection point on the surface

profile to determine the width. Nevertheless, the approximate measurement results match the theoretical calculation, and the simulations closely predict the channel geometry.

For the incomplete channel formation case in Fig. 13(*c*), corresponding to *Mode III* channels, given that the major overlapping ratio is only 0.61 and the minor overlapping ratio reaches 0.37, a blended dimple/channel surface topography is generated. The dimples overlap not only in the channel formation direction, but also between different channels, generating this unique pattern with reduced feature depth.

The experimental results, as expected, verify the concept of the spiral micro-channel generation process, however, there are two observations from the results that need to be addressed:

(1) The generated channels are not perfectly straight as predicted by the simulation. This is due to the unstable spindle rotation speed of the machine. This phenomenon is more prominent at the relatively low spindle speeds, where it was found that the channels display sinusoidal patterns, as shown in Fig. 14. This is predicted by adding a periodic variation to the spindle speed. If the variation is assumed to be in the form of a sine function, and the frequency and the peak-to-peak amplitude of this function are taken as 20 Hz and 2 RPM, the simulation results successfully capture the sinusoidal patterns of the channels. This observation points to the possibility to further extend the proposed method's capabilities in generating complex channel geometries, e.g., curved channels, by precise control of the spindle speed.

(2) The simulation tends to overpredict the channel or feature depth. This can be attributed to several reasons. One is possibly from the reduced vibration amplitudes while cutting. Since the vibration trajectories are recorded with no load, the system dynamics change when texturing dimples. The vibration amplitudes are very likely to be reduced due to the external resistance force (no position feedback of the tool motions is provided). The second possible reason is due to the complicated micro-cutting mechanics, because the cutting depth is so small, the ploughing and elastic recovery effects are not negligible and should be taken into account. This has been discussed partly in our previous work [23]. Another reason may be due to the motion error of the linear stage that sets a smaller *DOC* than the commanded one.

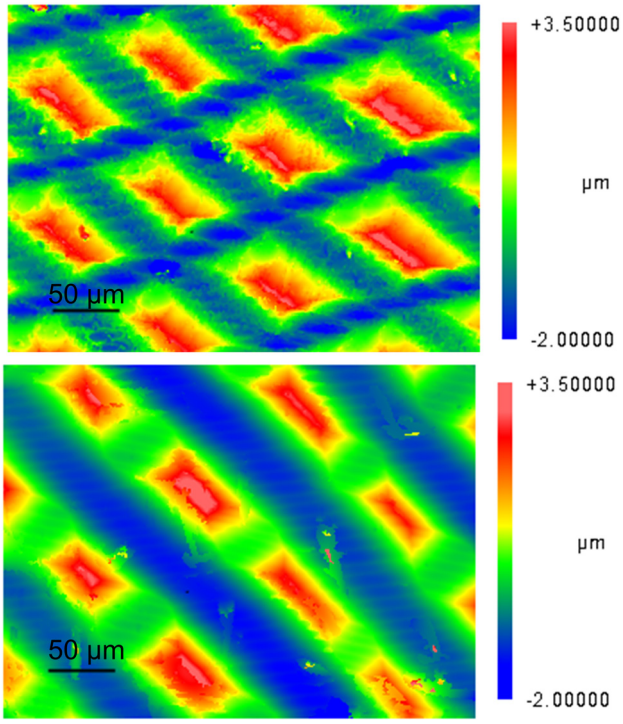

Fig. 15 Demonstration of micro-pattern generation

Crossing channels can also be created on the cylinder's surface, which results in micro-pattern generation, as shown in Fig. 15. *Mode II* channels were first created on the workpiece while the *Mode I* channels with a different orientation angle were overlaid on the existing textures to create pyramid-like shapes. This example shows the capabilities of this elliptical vibration texturing method for generating more complex patterns. If the cutting tool geometry is carefully designed, it is possible to generate desired patterns in very effectively in very short time using this method.

5 Conclusions

This paper has proposed the *elliptical vibration texturing* process for the generation of spiral micro-channels on cylindrical surfaces. The applications of such functional surfaces are usually for micro-fluidic devices, micro heat exchangers, and friction reduction. This newly developed method utilizes the tool's vibration to create modulations in the cutting depth. It was originally proposed by the authors to create micro-dimple arrays on cylindrical surfaces. Through the analysis, it was shown that micro-channels could be formed by overlapping the created dimples. This was achieved by carefully choosing the process parameters, i.e., the rotation speed and the feedrate.

There are three possible channel modes depending on the overlapping direction. The geometric analysis has been given in detail to relate channel formation to the overlapping ratios of the dimples in two directions, namely, along the channel and perpendicular to the channel. Thresholds on the overlapping ratios were set for channel formation. Thus, a channel generation map was created to relate the channel geometries and the process parameters.

Experimental results were provided to verify the analysis. It was first shown that the process is capable of producing dimple arrays as predicted. Second, based on the analysis of channel formation, the channels were successfully generated in the experiments using the calculated process parameters. The obtained geometric features are very close to the theoretical values and match the simulations quite well.

A discussion has been given on the curved shapes and reduced depth in the experimental results. The curved channels were due to the variation of the spindle speed. This feature has been also predicted from the simulation by adding a sinusoidal variation to the spindle speed. The reduced feature depth was attributed to be due to the system dynamics, micro-cutting mechanics, or the machine's motion error.

A further example of creation of micro-patterns using the elliptical vibration texturing process was also given, which shows the versatility of the process.

Acknowledgment

This work was supported by National Science Foundation under Grant number DMI-0600175 and the Korea Institute of Machinery & Materials (KIMM). The second author is also grateful to the financial support from the National Natural Science Foundation of China (Grant #51176082).

References

[1] Evans, C. J., and Bryan, J. B., 1999, ""Structured," "Textured" or "Engineered" Surfaces," CIRP Ann. 1999, **48**(2), pp. 541–556.
[2] Bruzzone, A. A. G., Costa, H. L., Lonardo, P. M., and Lucca, D. A., 2008, "Advances in Engineered Surfaces for Functional Performance," CIRP Ann., **57**(2), pp. 750–769.
[3] Li, X.-M., Reinhoudt, D., and Crego-Calama, M., 2007, "What Do We Need for a Superhydrophobic Surface? A Review on the Recent Progress in the Preparation of Superhydrophobic Surfaces," Chem. Soc. Rev., **36**(8), pp. 1350–1368.
[4] Suh, N. P., Mosleh, M., and Howard, P. S., 1994, "Control of Friction," Wear, **175**(1-2), pp. 151–158.

[5] Whitesides, G. M., 2006, "The Origins and the Future of Microfluidics," Nature, **442**(7101), pp. 368–373.
[6] Brandner, J. J., Anurjew, E., Bohn, L., Hansjosten, E., Henning, T., Schygulla, U., Wenka, A., and Schubert, K., 2006, "Concepts and Realization of Microstructure Heat Exchangers for Enhanced Heat Transfer," Exp. Thermal Fluid Sci., **30**(8), pp. 801–809.
[7] Kim, D. E., Cha, K. H., Sung, I. H., and Bryan, J., 2002, "Design of Surface Micro-Structures for Friction Control in Micro-Systems Applications," CIRP Ann., **51**(1), pp. 495–498.
[8] Hirayama, T., Sakurai, T., and Yabe, H., 2004, "A Theoretical Analysis Considering Cavitation Occurrence in Oil-Lubricated Spiral-Grooved Journal Bearings With Experimental Verification," J. Tribol., **126**(3), pp. 490–498.
[9] Sep, J., Pawlus, P., and Galda, L., 2013, "The Effect of Helical Groove Geometry on Journal Abrasive Wear," Arch. Civil Mech. Eng., **13**(2), pp. 150–157.
[10] Takeuchi, Y., Yoneyama, Y., Ishida, T., and Kawai, T., 2009, "6-Axis Control Ultraprecision Microgrooving on Sculptured Surfaces With Non-Rotational Cutting Tool," CIRP Ann., **58**(1), pp. 53–56.
[11] Holmes, A. S., Pedder, J. E., and Boehlen, K. L., 2006, "Advanced Laser Micromachining Processes for Mems and Optical Applications," p. 62611E.
[12] Groenendijk, M., 2013, "3D Surface Texturing Technology Using Ultrashort Pulsed Lasers," Laser Editorials, Laser Institute of America, http://www.lia.org/blog/2013/04/3d-surface-texturing-technology-using-ultrashort-pulsed-lasers/
[13] Hao, X., Wang, L., Wang, Q., Guo, F., Tang, Y., Ding, Y., and Lu, B., 2011, "Surface Micro-Texturing of Metallic Cylindrical Surface With Proximity Rolling-Exposure Lithography and Electrochemical Micromachining," Appl. Surf. Sci., **257**(21), pp. 8906–8911.
[14] Adams, D. P., Vasile, M. J., and Krishnan, A. S. M., 2000, "Microgrooving and Microthreading Tools for Fabricating Curvilinear Features," Precis. Eng, **24**(4), pp. 347–356.
[15] Li, G., Xu, Z., Fang, F., Wu, W., Xing, X., Li, W., and Liu, H., 2013, "Micro Cutting of V-Shaped Cylindrical Grating Template for Roller Nano-Imprint," J. Mater. Process. Technol., **213**(6), pp. 895–904.
[16] Lee, J. S., Lee, D. W., Jung, Y. H., and Chung, W. S., 2002, "A Study on Micro-Grooving Characteristics of Planar Lightwave Circuit and Glass Using Ultrasonic Vibration Cutting," J. Mater. Process. Technol., **130**, pp. 396–400.
[17] Liu, K., Li, X. P., Rahman, M., and Liu, X. D., 2004, "Study of Ductile Mode Cutting in Grooving of Tungsten Carbide With and Without Ultrasonic Vibration Assistance," Int. J. Adv. Manuf. Technol., **24**(5-6), pp. 389–394.
[18] Kim, G. D., and Loh, B. G., 2010, "Machining of Micro-Channels and Pyramid Patterns Using Elliptical Vibration Cutting," Int. J. Adv. Manuf. Technol., **49**(9-12), pp. 961–968.
[19] Suzuki, N., Yokoi, H., and Shamoto, E., 2011, "Micro/Nano Sculpturing of Hardened Steel by Controlling Vibration Amplitude in Elliptical Vibration Cutting," Precis. Eng., **35**(1), pp. 44–50.
[20] Brehl, D. E., and Dow, T. A., 2008, "Review of Vibration-Assisted Machining," Precis. Eng., **32**(3), pp. 153–172.
[21] Lu, X.-D., and Trumper, D. L., 2005, "Ultrafast Tool Servos for Diamond Turning," CIRP Ann., **54**(1), pp. 383–388.
[22] Guo, P., and Ehmann, K. F., 2013, "Development of a Tertiary Motion Generator for Elliptical Vibration Texturing," Precis. Eng., **37**(2), pp. 364–371.
[23] Guo, P., and Ehmann, K. F., 2013, "An Analysis of the Surface Generation Mechanics of the Elliptical Vibration Texturing Process," Int. J. Mach. Tools Manuf., **64**, pp. 85–95.
[24] Hong, M. S., and Ehmann, K. F., 1995, "Generation of Engineered Surfaces by the Surface-Shaping System," Int. J. Mach. Tools Manuf., **35**(9), pp. 1269–1290.
[25] Woronko, A., Huang, J., and Altintas, Y., 2003, "Piezoelectric Tool Actuator for Precision Machining on Conventional Cnc Turning Centers," Precis. Eng., **27**(4), pp. 335–345.
[26] Greco, A., Raphaelson, S., Ehmann, K., Wang, Q. J., and Lin, C., 2009, "Surface Texturing of Tribological Interfaces Using the Vibromechanical Texturing Method," ASME J. Manuf. Sci. Eng., **131**(6), pp. 061005.
[27] Moriwaki, T., and Shamoto, E., 1995, "Ultrasonic Elliptical Vibration Cutting," CIRP Ann., **44**(1), pp. 31–34.
[28] Shamoto, E., and Moriwaki, T., 1999, "Ultaprecision Diamond Cutting of Hardened Steel by Applying Elliptical Vibration Cutting," CIRP Ann., **48**(1), pp. 441–444.
[29] Zhang, X. Q., Kumar, A. S., Rahman, M., Nath, C., and Liu, K., 2011, "Experimental Study on Ultrasonic Elliptical Vibration Cutting of Hardened Steel Using Pcd Tools," J. Mater. Process. Technol., **211**(11), pp. 1701–1709.
[30] Suzuki, N., Haritani, M., Yang, J., Hino, R., and Shamoto, E., 2007, "Elliptical Vibration Cutting of Tungsten Alloy Molds for Optical Glass Parts," CIRP Ann., **56**(1), pp. 127–130.
[31] Nath, C., Rahman, M., and Neo, K. S., 2009, "A Study on Ultrasonic Elliptical Vibration Cutting of Tungsten Carbide," J. Mater. Process. Technol., **209**(9), pp. 4459–4464.
[32] Nath, C., Rahman, M., and Neo, K. S., 2011, "Modeling of the Effect of Machining Parameters on Maximum Thickness of Cut in Ultrasonic Elliptical Vibration Cutting," ASME J. Manuf. Sci. Eng., **133**(1), pp. 011007.
[33] Liang, Z., Wang, X., Wu, Y., Xie, L., Jiao, L., and Zhao, W., 2013, "Experimental Study on Brittle–Ductile Transition in Elliptical Ultrasonic Assisted Grinding (Euag) of Monocrystal Sapphire Using Single Diamond Abrasive Grain," Int. J. Mach. Tools Manuf., **71**, pp. 41–51.